Estimation of the Electron Thermalization Length in Ionic Materials

ARTICLE *in* JOURNAL OF PHYSICAL CHEMISTRY LETTERS · OCTOBER 2013

Impact Factor: 7.46 · DOI: 10.1021/jz401864w

THE JOURNAL OF PHYSICAL CHEMISTRY Letters

Letter

pubs.acs.org/JPCL

Estimation of the Electron Thermalization Length in Ionic Materials

Andrei Belsky,[†] Konstantin Ivanovskikh,[‡] Andrey Vasil'ev,[§] Marie-France Joubert,[†] and Christophe Dujardin*,[†]

[†]Institut Lumière Matière, UMR5306 Université Lyon 1-CNRS, Université de Lyon, 69622 Villeurbanne cedex, France

[‡]Department of Physics and Astronomy, University of Canterbury, Private Bag 4800, 8020 Christchurch, New Zealand

[§]Skobeltsyn Institute of Nuclear Physics, Lomonosov Moscow State University, Leninskie Gory 1(2), Moscow, 119991, Russia

ABSTRACT: We report estimations of the thermalization length and the diffusion coefficient of photogenerated carriers in the insulator $LiYF_4$ as a function of their initial energy. Combining modeling of electron−phonon interaction and the detailed analysis of the kinetic response of fluorescent center Ce^{3+} under vacuum ultraviolet excitation, the thermalization length is obtained as a function of the initial kinetic energy of the electron. This parameter is essential for the description of the carrier recombination in the case of nonideal plasma conditions, where electrons and holes are strongly correlated. This approach also demonstrates the effect of a complicated structure of electronic band on the thermalization process, which impacts the complex nonproportionality response of materials under ionizing radiation excitation.

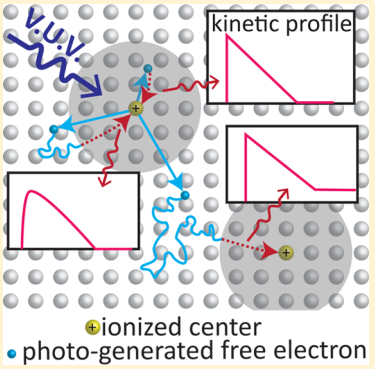

SECTION: Plasmonics, Optical Materials, and Hard Matter

A wide range of applications of optical materials are connected with their interaction with photons, the energy of which is higher than the forbidden gap of the material. The absorption of such a photon results in the production of an electron−hole pair, and the components of such pairs start to thermalize after the production. In the case of low intensity of exciting light, these pairs are not overlapped in space, and the probability of their recombination depends on the distance between these carriers after thermalization. Thermalization of carriers corresponds to the loss of kinetic energy mostly due to interaction with phonons, which drives their recombination probabilities. This effect is crucial in detectors of ionizing radiation, spectral transformers, and solar cells.[1,2] In particular, the geminate recombination (i.e., recombination of an electron and a hole produced by the same photon) influences the light yield and energy resolution of scintillators that are reaching the theoretical limit,[3−6] and is now discussed in the context of a wide number of applications such as homeland security, nuclear medical imaging, or calorimetry in high energy physics. This Letter presents a novel way of estimating essential physicochemical parameters that drive the electron transport in the conduction band and carrier recombination dynamics, namely, the diffusion coefficient and the thermalization length, which have so far remained uncharacterized in ionic materials.

While the initial stage of the electron−phonon relaxation has already been investigated in ionic systems in the picosecond regimes using pomp−probe experiments,[7,8] we now present a complete description of the process up to its end, i.e., the recombination of the carriers. The solution of such a problem of dynamics of ensemble of carriers, with large but finite number of carriers (far from both the thermodynamical limit and the two-particle system) is closely connected with the state-of-art of investigation of physicochemical principles of developing new materials. In this Letter, the data of vacuum utraviolet (VUV) time-resolved spectroscopic measurements are analyzed using a simplified theoretical model to estimate the dependence of the thermalization length as a function of the initial kinetic energy of an electron after ionization. To "probe" the thermalization process, a luminescent ion with fast (nanoseconds) fluorescence is used. Given that the discrete ground state of the probe ions lies in the forbidden bandgap, a monochromatic beam with the photon energy $h\nu$ higher than the ionization threshold energy (E_{thr}) of the probe ion can generate electrons with defined kinetic energy ($E_{kin} = h\nu - E_{thr}$). In reality, the initial energy of the electrons has a distribution with a width defined by the strength of electron−phonon interaction. The starting point (for thermalization) for these electrons is the position of the probe ion (Figure 1). Thermalization of the electrons with the energies $E_{kin} > k_BT$ results in a distribution of electrons around ionized centers, which is characterized by the thermalization length l_e. Whether the electron will be captured by the center or will escape from it, depends on the electron final location after thermalization. In the case of electron capture, the center is promoted to the excited state. Thermalization being a subpicosecond process,[9,10] it will not effect fluorescence kinetics, which is driven by the radiative transition rate of the emitting center, the distribution of distance "electron-ionized centers," and the diffusion

Received: September 2, 2013
Accepted: October 3, 2013

   dx.doi.org/10.1021/jz401864w | J. Phys. Chem. Lett. 2013, 4, 3534−3538

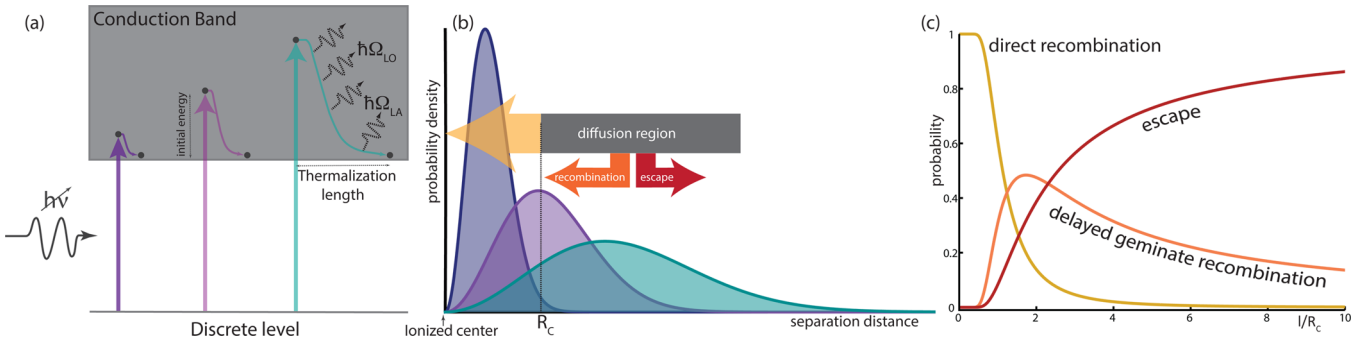

Figure 1. (a) Energy diagram representing the ionization of the discrete level of the probe ion located in the forbidden gap of ionic crystal by photons of various energies and the thermalization pathways of corresponding electrons in the conduction band. (b) Spatial distribution of thermalized electrons prior to diffusion for three illustrative initial kinetic energies according to eq 1. (c) Probability of three pathways for the electron after probe ion ionization as a function of initial electron location after thermalization obtained using the black sphere model for capture.

coefficient. Numerical analysis of the fluorescence kinetics as a function of the excitation energy provides information on the dependence of $l_e(E_{kin})$. Thermalization length of the electrons in ionic crystals has recently been estimated in ref 11; the approach is based on the well-known theory of electron−phonon interaction.[12−14] This theory predicts that the thermalization length increases with the electron initial kinetic energy E_{kin}. The account for interaction with longitudinal optical (LO) and acoustical (LA) phonons gives the analytical formula for $l_{e,LO}$ and $l_{e,LA}$ derived in ref 11. Given that thermalization stops when E_{kin} reaches k_BT, the probability to find thermalized electron at a certain distance from the ionized center c^+ can be written as a Gaussian in spherical coordinates:

$$f(r, l_e(E_{kin})) = \frac{3\sqrt{6}\,r^2}{\sqrt{\pi}\,l_e^3(E_{kin})} \exp\left(-\frac{3r^2}{2l_e^2(E_{kin})}\right) \quad (1)$$

Figure 1 illustrates the dependence of $f(r,l_e(E_{kin}))$ for various l_e. The thermalization process is hardly affected by the Coulomb interaction between the electron and the ionized center c^+, when the kinetic energy of the electron is larger than the Coulomb potential; however, the Coulomb potential becomes important for the diffusion of thermalized carriers. Such recombination results in the creation of excited state of the emission center c^*. For the electron behavior driven by the Coulomb potential and the diffusion processes, we use the Onsager model.[15] If the thermalized electron is located at the distance r from c^+, it recombines with the center with the probability $1 - e^{-R_{Ons}/r}$; it escapes from the center with the probability of $e^{-R_{Ons}/r}$. The Onsager radius R_{Ons} corresponds to the distance for which the thermal energy is equal to the Coulomb potential energy, thus by definition $R_{Ons} = (e^2/(4\pi\varepsilon_0\varepsilon_{st}k_BT))$ (ε_{st} being the relative static dielectric permittivity of the medium); R_{Ons} is about 10 nm at room temperature in ionic materials. At large distances, the recombination probability decreases as R_{Ons}/r. To perform the fitting procedure, we approximate the Onsager approach to a capture black sphere model of critical radius $R_c = R_{Ons}$. For electrons at distance r from the ionized center at $t = 0$, the probability to recombine is 1 for $r < R_c$; this recombination resulting in the creation of the excited state is considered instantaneous. For $r > R_c$, the probability of recombination with the geminate center decreases as R_c/r. In this case, the drift toward the virtual black sphere is controlled by the diffusion, and hence the recombination is delayed. In all other cases, the electron escapes its geminate ionized center and can recombine with another alien ionized center (nongeminate recombination). Given the initial spatial distribution of electrons after thermalization with a diffusion length l_e, we can calculate various probabilities of direct and delayed electron recombination as well as the probability of escape (Figure 1). Fluorescence kinetics is controlled by the evolution of the excited state population for the center n_{c*}, the equation of which is $((\partial n_{c*})/\partial t) = -((n_{c*})/\tau) + ((\partial n_{c+})/\partial t)$. Direct recombination ($r < R_c$) leads to an exponential fluorescence decay with a time constant τ, which depends on the radiative and nonradiative recombination rates of the considered center. This value can easily be obtained experimentally by direct excitation of the center. If Δn is the concentration of $e-c^+$ pairs created by one excitation pulse, the concentration of excited centers produced after direct recombination equals

$$n_{c^*} = \Delta n\left[\mathrm{erf}\left(\sqrt{\frac{3}{2}}\frac{R_c}{l_e}\right) - \sqrt{\frac{6}{\pi}}\frac{R_c}{l_e}\exp\left(-\frac{3R_c^2}{2l_e^2}\right)\right] \quad (2)$$

The radiative recombination on the geminate center for $r > R_c$ is controlled by the diffusion coefficient. Considering the evolution of the spatial distribution due to diffusion starting at $t = 0$ (eq 1), the flux of electrons entering the capture black sphere can be estimated as a function of time. This allows estimating the evolution of population of the ionized centers with time, which corresponds to an increase of the excited center population that leads to a radiative decay:

$$n_{c^+} = \Delta n\left[1 - \mathrm{erf}\left(\sqrt{\frac{3}{2}}\frac{R_c}{l_e}\right)\right] + \sqrt{6}\,\Delta n\frac{R_c}{\sqrt{\pi(l_e^2 + 6D_et)}} \exp\left(-\frac{3R_c^2}{2(l_e^2 + 6D_et)}\right) \times \left[1 - \mathrm{erf}\left(\frac{3R_c}{l_e}\sqrt{\frac{D_et}{l_e^2 + 6D_et}}\right)\right] \quad (3)$$

D_e is the electron diffusion coefficient. Only part of the ionized centers recombine with their geminate electrons, and for long times ($t \gg l_e^2/D_e$), the concentration of ionized centers remains equal to

$$n_{c^+}^{\infty} = \Delta n\left[1 - \mathrm{erf}\left(\sqrt{\frac{3}{2}}\frac{R_c}{l_e}\right)\right] \quad (4)$$

Nongeminate recombination also contributes to the time dependence of the probe fluorescence. Diffusion processes define the dynamic behavior, which depends on the

dx.doi.org/10.1021/jz401864w | J. Phys. Chem. Lett. 2013, 4, 3534−3538

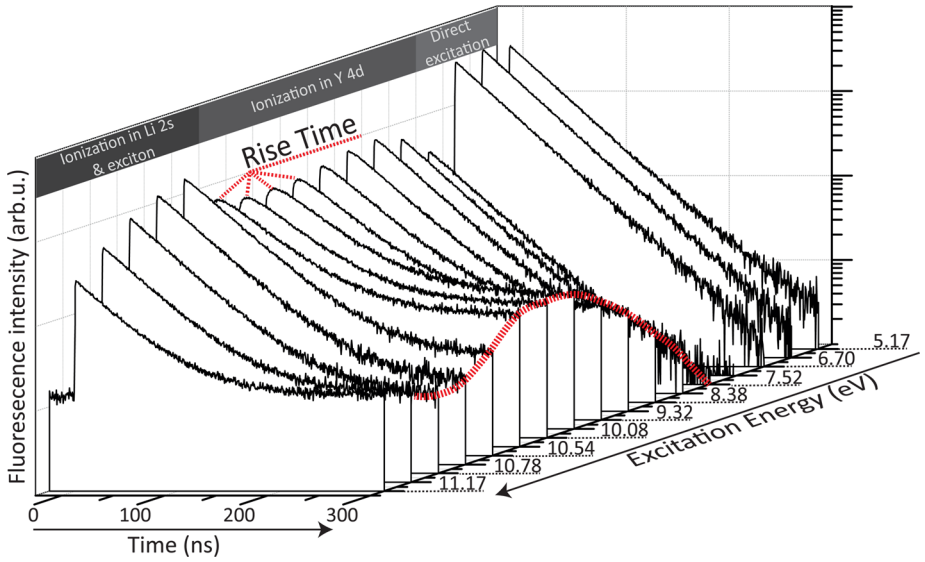

Figure 2. Fluorescence decay curves of $LiYF_4:Ce^{3+}$ for different excitation energies from 5.17 to 11.17 eV. The red line is a guide to the eye to point out the occurrence of the slow component for excitation energies above 8 eV. The curves with substantial rise-on regions are also indicated. Three regions of interest (direct excitation−ionization to the Y4d and to Li2s as well as exciton formation) are mentioned.

concentration of ionized centers and of electrons escaping geminate recombination. Thus the fluorescence kinetics depends on the excitation power density, concentration of ionized centers, of neutral centers, and of noncorrelated pair "electron-ionized centers" n_{nc}. Free electrons and ionized centers can recombine in a stochastic way leading to the time evolution (for $t \gg l_e^2/D_e$):

$$n_{c^+} = n_{c^+}^{\infty} \exp\left(-4\pi D_e R_c \left(t + \frac{2R_c}{\sqrt{\pi D_e}}\sqrt{t}\right) n_{nc}\right) \quad (5)$$

The interplay between geminate and nongeminate recombination is manifested as a rise time and a slow component in the fluorescence decay of the probe. The rise time corresponds to the mean migration time before geminate recombinations, the slow component being due to nongeminate recombinations. Accurate fitting of the decay curves yields an estimation of the thermalization length as a function of the initial kinetic energy of the electrons and the diffusion coefficient D_e.

To apply this model, the ionic crystal $LiYF_4$ doped with Ce^{3+} has been investigated. Ce^{3+} is known to exhibit fast parity-allowed radiative transitions $5d^1 \rightarrow 4f^1$. In this crystal, the fluorescence decay time of Ce^{3+} centers has been estimated to be τ = 28 ns at liquid helium temperature,[16] which is well-adapted to use this emission center as a probe for the thermalization length. The discrete ground state of Ce^{3+} lies in the $LiYF_4$ forbidden bandgap and the Ce^{3+} 5d bands can be excited in the UV range leading to the emission at 320 nm.[17,18] We measured the fluorescence decay curves of Ce^{3+} using excitation energies between 5.2 and 11.2 eV at the SUPERLUMI station of synchrotron radiation facility HASYLAB at DESY.[19] A series of fluorescence decay curves is presented in Figure 2. When excitation energy corresponds to the intracenter excitation of Ce^{3+}, the decay is described by a single exponential. For higher energies (>6 eV), ionization of cerium ion occurs with well-defined initial kinetic energy of the electron and rise-on times, and slow components appear in the fluorescence decay kinetics. The curves were fitted with the account for the repetition rate of the excitation pulses and the instrument timing properties, which enables us to obtain the ratio R_c/l_e as a function of the excitation energy. As described above, the Onsager radius depends on the dielectric constant of the medium and on the temperature. In the case of $LiYF_4$, ε_{st} has been obtained using infrared reflectivity.[20,21] In one case, authors found ε_{st} = 7.8 while Macedo et al. obtained 8 and 12 due to anisotropy. Assuming ε_{st} = 8 gives the R_{Ons} = 7 nm at room temperature, which allows us to plot the thermalization length as a function of the excitation energy (squares in Figure 3). From the fitting we also deduce the diffusion coefficient D_e

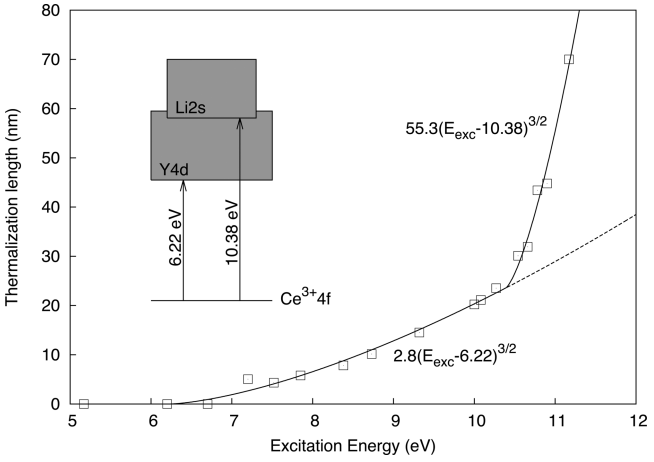

Figure 3. Dependence of the thermalization length on the excitation energy. Solid line corresponds to the best fit considering a model with two ionization thresholds according to $l_{e,Io}(E_{ph}) \propto 1/m_e^*(E_{ph} - E_{thr})^{3/2}$.

= 0.5 × 10^{-3} cm^2/s. The diffusion coefficient measured in the present paper includes the effect of potiential intermediate trapping of the carrier; the relatively small value of this diffusion coefficient indicates that this effect remains small.

In order to analyze the data presented in Figure 3, a model described in[11] is used. In this reference the dependence of the thermalization length on the initial kinetic energy and phonon energies was obtained. This result clearly indicates two stages of

dx.doi.org/10.1021/jz401864w | J. Phys. Chem. Lett. 2013, 4, 3534−3538

interaction with the LO and LA phonons. At high energies, the thermalization is mainly due to the interaction with LO phonons. This statement is valid down to kinetic energies equal to the lowest LO phonon energy. Below this limit, emission of LO phonon cannot occur and is replaced by the interaction with LA phonons. We can thus consider two separate thermalization lengths l_{LO} and l_{LA}, contributing separately to define the overall thermalization length. When originating from the ionization of a dopant ion, thermalization of the electron occurs in the vicinity of the ionized center. The Onsager model is valid for thermalized electrons (i.e., for an electron with kinetic energy around k_BT). We can thus separate the whole process of relaxation into thermalization (i.e., the process when kinetic energy decreases down to k_BT) and recombination. During the first one (thermalization), we neglect the Coulomb interaction, whereas during the second one (capture or recombination) we neglect the changes of electron kinetic energy, which is about k_BT. Therefore, if the material has its smallest LO phonon energy bellow k_BT, one can approximate the electron thermalization length as l_{LO}. $LiYF_4$ has a complicated phonon band structure with many phonon branches. Several LO modes with the energy below 200 cm^{-1} (k_BT at room temperature) were observed by Raman and infrared spectroscopy.[22] The dependence on the excitation energy is described in ref 11. In the case of $E_{kin} \gg \hbar\,\Omega_{LO}$, the formula for the thermalization length obtained in[11] can be used as $l_{e,LO}(E_{ph}) \propto 1/m_e^*(E_{ph} - E_{thr})^{3/2}$. We fitted the experimental data using this model. The results presented in Figure 3 reveal a significant slope change around 10.5 eV, indicating that a single ionization threshold cannot be used. We thus used a model with two ionization thresholds, which is consistent with the complicated conduction band structure comprising the Y4d orbitals as well as the Li2s ones at higher energy.[23] The fitting procedure gives the energy separation for Ce^{3+}4f-Y4d and Ce^{3+}4f-Li2s as 6.22 and 10.38 eV, respectively. Based on the simplified equation presented above, the fitting parameters indicate that the ratio of effective masses of Y4d and Li2s electrons is about 20. To verify this estimate, comparison with the band structure calculations of $LiYF_4$ as well as with a simpler crystal having a conduction band composed of Li2s orbitals (LiF) is considered.[24,25] The ratio of effective masses m_e^* between Y4d and Li2s electrons is then found between 3 to 8, which is lower than 20 derived from our fitting procedure. Nevertheless, this large value reflects a property of the Y4d and Li2s dispersion curves. Indeed, the effective mass depends on the crystal structure itself and electronic band calculations are also subject to approximation. The additional proportionality factor to take into account is the square of the transition matrix element for electron−phonon interaction. This factor is less for transitions within the Y4d subbands than for the Li2s subbands since there is additional orthogonality of states within the Y4d multiplets. At excitation energies above 10.5 eV an additional effect should be considered, namely, the formation of F2p-Y4d exciton. There is a substantial overlap between excitonic emission (220 to 400 nm at low temperature[26]) and Ce^{3+} 4f-5d absorption allowing for efficient dipole−dipole energy transfer. The exciton at RT is quenched, and its characteristic decay time is less than nanoseconds. The energy transfer from the exciton to cerium is efficient even for thermally quenched excitons, since this transfer occurs only for excitons located within R_{d-d} radius around the cerium ion and occurs in the subnanosecond time domain. This transfer mechanism remains effective up to temperatures for which the thermally quenched exciton lifetime reaches this time domain. Ce^{3+} excitation via energy transfer from the exciton yields a substantial fraction of instantaneous cerium excitation. The contribution from cerium absorption in the fundamental absorption region is small, the fraction of ionization processes that we considered above is reduced substantially, making it difficult to subtract its contribution. Though above 10.5 eV the error in the estimation of the thermalization length is bigger than in transparency region, we still assign the change in the slope at this energy to the increased thermalization length related to the Li2s band.

In conclusion, using a detailed analysis of the fluorescence kinetics of an activator in its photoionization regime, we were able to estimate the thermalization length of an electron as a function of its kinetic energy in the case of $LiYF_4$. The numerical value increases up to 20 nm for a kinetic energy of 3 eV. For higher kinetic energies, the effect of the Li2s band is demonstrated and the thermalization length increases rapidly up to 70 nm for a small increase of the kinetic energy from 3 eV to 4 eV. Furthermore, the applied procedure allows to deduce a diffusion coefficient of $D = 0.5 \times 10^{-3} cm^2\ s^{-1}$. These numerical estimations can serve as input parameters in Monte Carlo simulations of the charge relaxation in such a materials. In addition to that, the method can be extend to other materials as long as doping ions exhibiting a fast luminescence can be introduced.

AUTHOR INFORMATION

Corresponding Author

*E-mail: christophe.dujardin@univ-lyon1.fr.

Notes

The authors declare no competing financial interest.

ACKNOWLEDGMENTS

The authors acknowledge fruitful discussions with Dr. I. A. Kamenskikh. The work was partially supported by the Project FP7-INCO-2011-6 “SUCCESS”.

REFERENCES

(1) Pensack, R.; Asbury, J. Beyond the Adiabatic Limit: Charge Photogeneration in Organic Photovoltaic Materials. *J. Phys. Chem. Lett.* **2010**, *1*, 2255−2263.

(2) Shafran, E.; Borys, N.; Huang, J.; Talapin, D.; Lupton, J. Indirect Exciton Formation due to Inhibited Carrier Thermalization in Single CdSe/CdS Nanocrystals. *J. Phys. Chem. Lett.* **2013**, *4*, 691−697.

(3) Li, Q.; Grim, J.; Ucer, K.; Burger, A.; Bizarri, G.; Moses, W.; Williams, R. Host Structure Dependence of Light Yield and Proportionality in Scintillators in Terms of Hot and Thermalized Carrier Transport. *Phys. Status Solidi RRL* **2012**, *6*, 346Ð348.

(4) Williams, R.; Grim, J.; Li, Q.; Ucer, K.; Moses, W. Excitation Density, Diffusion-Drift, and Proportionality in Scintillators. *Phys. Status Solidi B* **2011**, *248*, 426−438.

(5) Payne, S.; Cherepy, N.; Hull, G.; Valentine, J.; Moses, W.; Choong, W. Non-Proportionality of Scintillator Detectors: Theory and Experiment. *IEEE Trans. Nucl. Sci.* **2009**, *NS-56*, 2506−2512.

(6) Vasil'ev, A. From Luminescence Non-linearity to Scintillation Non-proportionality. *IEEE Trans. Nucl. Sci.* **2008**, *55*, 1054−1061.

(7) Quere, F.; Guizard, S.; Martin, P.; Petite, G.; Merdji, H.; Carre, B.; Hergott, J.; Le Deroff, L. Hot-Electron Relaxation in Quartz Using High-Order Harmonics. *Phys. Rev. B* **2000**, *61*, 9883−9886.

(8) Mao, S.; Quere, F.; Guizard, S.; Mao, X.; Russo, R.; Petite, G.; Martin, P. Dynamics of Femtosecond Laser Interactions with Dielectrics. *Appl. Phys. A: Mater. Sci. Process.* **2004**, *79*, 1695−1709.

(9) Quere, F.; Guizard, S.; Martin, P. Time-Resolved Study of Laser-Induced Breakdown in Dielectric. *Europhys. Lett.* **2001**, *56*, 138−144.

(10) Martin, P.; Guizard, S.; Daguzan, P.; Petite, G.; D'Oliveira, P.; Meynadier, P.; Perdrix, M. Subpicosecond Study of Carrier Trapping Dynamics in Wide-Band-Gap Crystals. *Phys. Rev. B* **1997**, *55*, 5799−5810.
(11) Kirkin, R.; Mikhailin, V. V.; Vasil'ev, A. N. Recombination of Correlated Electron-Hole Pairs With Account of Hot Capture With Emission of Optical Phonons. *IEEE Trans. Nucl. Sci.* **2012**, *59*, 2057−2064.
(12) Frohlich, H. Electrons in Lattice Fields. *Adv. Phys.* **1954**, *3*, 325−361.
(13) Llacer, J.; Garwin, E. Electron-Phonon Interaction in Alkali Halides 0.1. Transport of Secondary Electrons with Energies between 0.25 and 7.5 eV. *J. Appl. Phys.* **1969**, *40*, 2766−2775.
(14) Sparks, M.; Mills, D.; Warren, R.; Holstein, T.; Maradudin, A.; Sham, L.; Loh, E.; King, D. Theory of Electron-Avalanche Breakdown in Solids. *Phys. Rev. B* **1981**, *24*, 3519−3536.
(15) Onsager, L. Initial Recombination of Ions. *Phys. Rev.* **1938**, *54*, 554−557.
(16) Kirikova, N.; Kirm, M.; Krupa, J.; Makhov, V.; Negodin, E.; Gesland, J.; Low-Temperature High-Resolution, V. U. V. Spectroscopy of Ce^{3+} Doped $LiYF_4$, $LiLuF_4$ and LuF_3 Crystals. *J. Lumin.* **2004**, *110*, 135−145.
(17) Dorenbos, P.; Dorenbos, P. The $4f^n \leftrightarrow 4f^{n-1}5d$ Transitions of the Trivalent Lanthanides in Halogenides and Chalcogenides. *J. Lumin.* **2000**, *91*, 91−106.
(18) Blanc, W.; Dujardin, C.; Gacon, J.; Pedrini, C.; Moine, B.; A.N., B.; Kamenskikh, I.; Kirm, M.; Zimmerer, G. On the Role of the 4f-Lu Level in the Scintillation Mechanisms of Cerium-Doped Lutetium-Based Fluoride Crystals. *Radiat. Eff. Defects Solids* **1999**, *150*, 41−46.
(19) Zimmerer, G. SUPERLUMI: A unique setup for luminescence spectroscopy with synchrotron radiation. *Radiat. Meas.* **2007**, *42*, 859−864.
(20) Miller, S.; Rast, H.; Caspers, H. Lattice Vibrations of $LiYF_4$. *J. Chem. Phys.* **1970**, *52*, 4172−4175.
(21) Macedo, R.; Dumelow, T. Beam Shifts on Reflection of Electromagnetic Radiation off Anisotropic Crystals at Optic Phonon Frequencies. *J. Opt.* **2013**, *15*, 014013.
(22) Salaun, S.; Fornoni, M.; Bulou, A.; Rousseau, M.; Simon, P.; Gesland, J. Lattice Dynamics of Fluoride Scheelites 0.1. Raman and Infrared Study of $LiYF_4$ and $LiLnF_4$ (Ln = Ho, Er, Tm and Yb). *J. Phys: Condens. Matter* **1997**, *9*, 6941−6956.
(23) Yin, J.; Hang, Y.; Zhang, L. Ab Initio Calculations of Electronic Structures of $LiYF_4$ Crystals Containing F-Type Color Centers. *Opt. Mater.* **2009**, *32*, 194−197.
(24) Curtarolo, S.; Setyawan, W.; S., W.; Xue, J.; Yang, K.; Taylor, R.; Nelson, L.; Hart, G.; Sanvito, S.; Buongiorno-Nardelli, M.; Mingo, N.; Levy, O. AFLOWLIB.ORG: A Distributed Materials Properties Repository from High-Throughput Ab Initio Calculations. *Comput. Mater. Sci.* **2012**, *58*, 227−235.
(25) Setyawan, W.; Curtarolo, S. High-Throughput Electronic Structure Calculations: Challenges and Tools. *Comput. Mater. Sci.* **2010**, *49*, 299−312.
(26) Hayes, W.; Yamaga, M.; Robbins, D.; Cockayne, B. Optical Detection of Exciton EPR in $LiYF_4$. *J. Phys. C: Solid State Phys.* **1980**, *13*, L1011−5.